Excitation intensity dependence of photoluminescence spectra of SiGe quantum dots grown on prepatterned Si substrates: Evidence for biexcitonic transition

P. Klenovský,[1,2,*] M. Brehm,[3] V. Křápek,[1,4] E. Lausecker,[3] D. Munzar,[1,2] F. Hackl,[3] H. Steiner,[3] T. Fromherz,[3] G. Bauer,[3] and J. Humlíček[1,2]

[1]*Department of Condensed Matter Physics, Faculty of Science, Masaryk University, Kotlářská 2, 61137 Brno, Czech Republic*
[2]*CEITEC–Central European Institute of Technology, Masaryk University, Kamenice 753/5, 62500 Brno, Czech Republic*
[3]*Institute of Semiconductor and Solid State Physics, Johannes Kepler University Linz, 4040 Linz, Austria*
[4]*Institute of Physics, Academy of Sciences of the Czech Republic, Cukrovarnická 10, Praha 6, 162 53 Czech Republic*

(Received 14 May 2012; published 4 September 2012)

The pumping intensity (I) dependence of the photoluminescence (PL) spectra of perfectly laterally two-dimensionally ordered SiGe quantum dots on Si(001) substrates was studied. The PL results from recombinations of holes localized in the SiGe quantum dots and electrons localized due to the strain field in the surrounding Si matrix. The analysis of the spectra revealed several distinct bands, attributed to phonon-assisted recombination and no-phonon recombination of the excitonic ground state and of the excited excitonic states, which all exhibit a linear I dependence of the PL intensity. At approximately $I \geqslant 3$ W cm^{-2}, additional bands with a nearly quadratic I dependence appear in the PL spectra, resulting from biexcitonic transitions. These emerging PL contributions shift the composite no-phonon PL band of the SiGe quantum dots to higher energies. The experimentally obtained energies of the no-phonon transitions are in good agreement with the exciton and biexciton energies calculated using the envelope function approximation and the configuration interaction method.

DOI: 10.1103/PhysRevB.86.115305 PACS number(s): 73.21.La, 73.22.Lp, 78.55.Ap, 78.67.Hc

I. INTRODUCTION

SiGe quantum dots (QDs) are of interest, since they provide a promising way towards an infrared light source operating on telecom wavelengths, integrable into the present Si-based technology.[1] Although these structures have been studied for quite a long time,[2,3] there are only a few reports on the excitonic structure of their photoluminescence (PL) spectra.[4–6] The large size of the QDs and an inhomogeneous Ge distribution due to intermixing and clustering lead to a pronounced broadening of the PL lines of QD ensembles.[7] Additional broadening arises from the indirect nature of the optical transitions both in real and reciprocal space. Due to the broad spectra, an unambiguous assignment of the electronic QD transitions of randomly nucleated QDs grown on planar Si(001) has not been reported so far. For the same reasons, up to now only continuous linear and sublinear shifts of the PL emission energies with increasing excitation intensity (I) could be observed both for SiGe QDs (Refs. 8 and 9) and quantum wells (QWs),[10–12] which were attributed to state filling effects and carrier-induced band bending as a consequence of the spatial separation of the excited electrons and holes.

It has been shown that by a precise positioning of the QDs on prestructured Si substrates,[13] a significant narrowing of the PL spectra can be achieved,[7,14–16] making a more detailed analysis of the dependence of the PL spectra on the excitation intensity possible. However, no decomposition of the PL spectra in terms of individual excitonic recombinations has been reported so far for laterally ordered SiGe QDs. Here we provide an identification of both bound excitonic and biexcitonic transitions in the PL spectra of ensembles of ordered SiGe QDs, using the linear and quadratic excitation intensity dependence of those transitions. This identification is facilitated by the clear observation of additional PL emission lines that appear with increasing I at higher photon energies as opposed to the continuous shift of the PL spectra reported up to now. The assignments are supported by the results of exciton and biexciton energy level calculations.

Extensive work on the exciton-exciton interaction energies has been reported for self-assembled epitaxial III-V compound quantum dots[17–22] as well as for chemically synthesized colloidal nanocrystals[23–25] for material systems with both type-I and II band alignment. The understanding of the multiexciton interaction and the exciton relaxation dynamics has been shown to be important for the realization of hot carrier extraction and optical gain.[25,26]

In this work the exciton-exciton interaction as well as the exciton excited-state energies are determined experimentally for SiGe QDs epitaxially embedded in a Si matrix. In this material system, the holes are confined in the SiGe QDs and the electrons to the tensile strained regions in the Si matrix surrounding them, forming a type-II system. Our results show that for the ordered, highly uniform SiGe QDs investigated in this work, the energy splitting between the biexciton and exciton emission line is larger than the linewidth, which is a prerequisite to achieve optical gain for single exciton states.[26]

This paper is organized as follows: In Sec. II, experimental details on SiGe island growth and on the PL measurements are presented. In Sec. III, the analysis of the PL spectra, their excitation intensity dependence, electronic structure calculations, and the resulting assignment of the exciton, excited exciton, biexciton, and excited biexciton energies are given. In Sec. IV, the conclusions are presented.

II. EXPERIMENT

Two samples with different average Ge content in the SiGe QDs were investigated ($S1$ and $S2$). High resistivity p-type Si (001) substrates were pit patterned by nanoimprint lithography and subsequent pattern transfer into the substrate by reactive ion etching. The pattern periods were 300 nm for

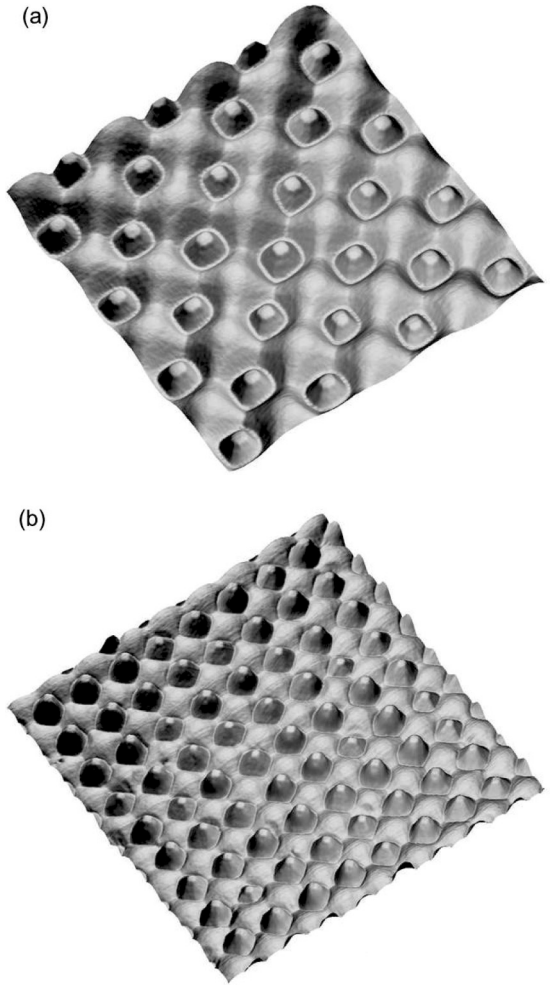

FIG. 1. Atomic force micrographs of the samples (a) $S1$ (pit period 300 nm) and (b) $S2$ (pit period 170 nm). The scanned area was 1.5×1.5 μm for both samples. The average height of the QDs in sample $S1$ ($S2$) is 15.3 (15) nm and the QD base diameter is 122.8 (118) nm.

$S1$ and 170 nm for $S2$, and the patterned areas were 3×3 mm^2 for both samples. The resulting pits had diameters and depths of 160 and 47 nm for $S1$, and 120 and 35 nm for $S2$, respectively. After standard cleaning, the wafers were *in situ* degassed in the solid source molecular beam epitaxy chamber for 40 min at 720 °C. Hereafter, a 45-nm-thick Si buffer layer (growth rate $R = 0.6$ Å/s) was deposited at a substrate temperature that was increased from 450 °C to 550 °C followed by the deposition of six monolayers (ML) of Ge at 690 °C ($R = 0.05$ Å/s) for $S1$ and 8.3 ML of Ge at 625 °C ($R = 0.025$ Å/s) for $S2$. Subsequently, a 50- or a 10-nm-thick Si capping layer was deposited at a temperature as low as 300 °C in order to avoid unwanted Si incorporation and QD shape transformations for $S1$ or $S2$, respectively.[27] Atomic force micrographs of the ordered and capped islands are shown in Fig. 1 for $S1$ and $S2$.

In the PL measurements, performed at 4.2 K, the samples were excited by an Ar^+ laser tuned to the wavelength of 457.9 nm, focused by a lens to a circular area with 400-μm-diameter ($\sim 10^6$ irradiated QDs). The excitation intensities ranged from 0.15 to 7.90 W cm^{-2} for sample $S1$ and from 0.15 to 3.95 W cm^{-2} for sample $S2$. After being dispersed by a grating monochromator, the PL light was detected using an InGaAs line detector at the temperature of −100 °C.

III. RESULTS AND DISCUSSION

A. Analysis of the photoluminescence spectra

In Figs. 2(a)–2(c) the PL spectra of $S1$ are shown for three excitation intensities ($I = 0.25$, 0.49, and 4.94 W cm^{-2}) together with their decomposition into various lines according to the fitting procedure described below. It is evident that with increasing I additional lines appear in the high-energy shoulder of the PL spectra. The observed behavior cannot be described by a continuous shift of the emission energy caused

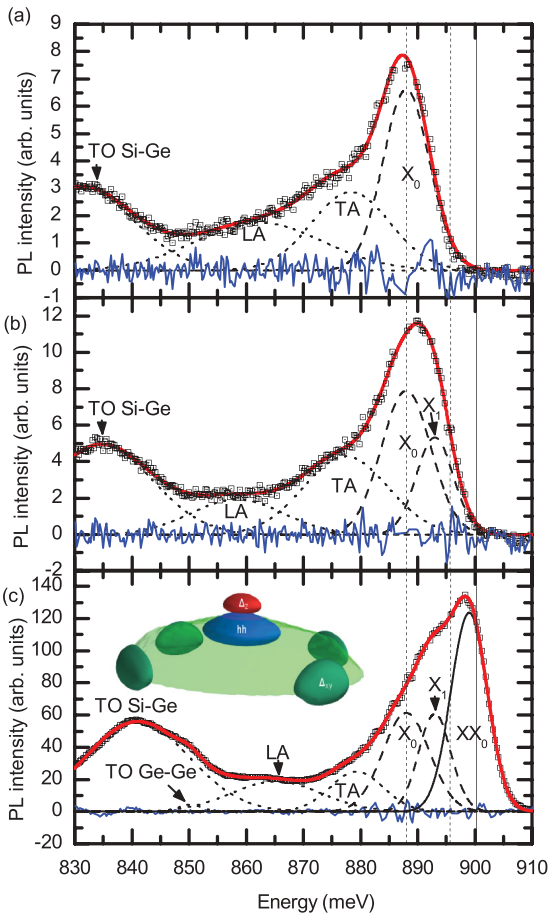

FIG. 2. (Color online) Measured (open squares) and fitted (red curve) PL spectrum of the sample $S1$ for (a) $I = 0.25$ W cm^{-2}, (b) $I = 0.49$ W cm^{-2}, and (c) $I = 4.94$ W cm^{-2}. The residual error (blue curve) has been multiplied by a factor of 2. The individual GL profiles are attributed to phonon replicas (dotted curves), excitonic (X_0, X_1, broken curves), and biexcitonic (XX_0, full curve) states. The calculated values of the energies of the excitonic (biexcitonic) states for the model dome-shaped dot (see Fig. 5) blueshifted by 1 meV are displayed by dashed (solid) vertical lines. The inset of panel (c) shows the calculated probability densities (contours of $|\Psi^2| = 0.1$ nm^{-3}) of the hole ground state (blue), Δ_{xy} (green), and Δ_z (red) electron ground states and their location within the dot (its surface is represented by the light green surface) as obtained by the nextnano++ simulation suite (Ref. 31).

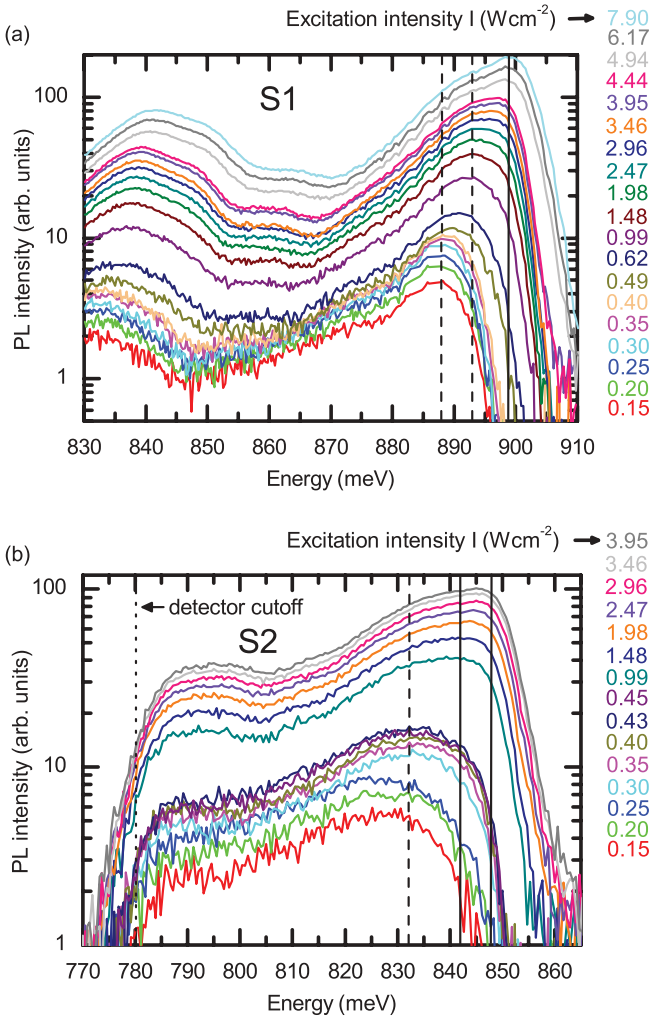

FIG. 3. (Color) Measured PL spectra (the values of the pumping intensity are given next to the right vertical axis) for samples (a) $S1$ and (b) $S2$. Dashed (solid) vertical lines correspond to the resonance energies E_0 of the fitted GL profiles attributed to excitons (biexcitons). The dotted vertical line in (b) corresponds to the detector cutoff energy of 780 meV.

by band bending as a consequence of electron-hole separation due to the type-II band alignment in the SiGe QDs. For the complete range of excitation intensities the PL spectra of $S1$ and $S2$ are shown on a logarithmic scale in Fig. 3. Due to the lower growth temperature for the islands in sample $S2$ as compared to $S1$, both the average and the maximum Ge content in $S2$ are larger.[7] Thus, the island-related PL spectrum of $S2$ is observed at lower energies than for $S1$. For both samples, the appearance of additional lines with increasing I (as shown in detail in Fig. 2) is evident over an excitation intensity range between 0.15 and 7.9 (3.95) W cm^{-2} for $S1$ ($S2$). In the following, a quantitative description of our observations in terms of excitonic contributions will be given.

In order to identify the transitions contributing to the individual PL spectra as a function of I, the spectra were fitted using the Gauss-Lorentz (GL) profiles, employing the method of the rational approximants.[28] Three parameters were used to describe each contribution: the resonant energies ($E_{0,i}$), the oscillator strengths (F_i), and the Gaussian widths ($\Gamma_{G,i}$), where i indexes the GL profiles. For the spectral region of phonon replicas below 885 meV (828 meV) for $S1$ ($S2$) (see also Fig. 2), the values of all these parameters were adjusted to fit the data, while for the region of no-phonon transitions the values of $E_{0,i}$ were fixed and only those of F_i and $\Gamma_{G,i}$ allowed to vary in the fitting routine. The fixing of the values of $E_{0,i}$ has been motivated by our experimental finding that in the no-phonon region the lines indeed appear at $E_{0,i}$ and are fitted more precisely with increasing I. This is in agreement with the assumption that every profile in the region of no-phonon transitions corresponds to one excitonic or biexcitonic transition. The width of the Lorentzian contributions $\Gamma_{L,i}$ to the fitted linewidth was fixed at the small value of 0.001 meV for all the fitted GL profiles, i.e., the profiles were treated as almost purely Gaussian ones. The Lorentzian width is negligible at low temperatures because the dominant spectral broadening is inhomogeneous, originating mainly in the statistical variation of the QD structure.

We have fitted every PL spectrum using the smallest number of profiles needed for a reasonably good fit, assessed by the residual sum of squares and the correlation coefficients between the fitted parameters. The values of the parameters obtained for I_n were used as starting values for fitting the spectrum measured at I_{n+1}. Here I_n and I_{n+1} denote subsequent excitation intensities in the series shown in Fig. 3. If, for the given number of profiles the best agreement at I_{n+1} was significantly worse than that at I_n, an additional profile was added. In this manner we have identified, for both samples, the number of profiles of the phonon-assisted part of the spectra to be three or four, and the number of the no-phonon part ranging from one to three. As an example, we show in Fig. 2 three selected PL spectra of the sample $S1$ along with the decomposition into the individual GL profiles. The values of $E_{0,i}$ are summarized in Table I.

The phonon-assisted transitions were attributed to the various SiGe phonon modes typically observed in the PL spectra of bulk SiGe samples[29] and quantum wells.[30] With increasing value of E_0 these are the Si-Ge transverse optical (TO), the Ge-Ge TO (for $S1$ resolved only at $I > 1.48$ W cm^{-1}), the longitudinal acoustic (LA), and the transverse acoustic (TA) (for $S2$ resolved only at $I > 0.20$ W cm^{-1}) phonon-assisted transitions. The Si-Si TO phonon-assisted transition was not identified in our spectra; its contribution may overlap with the band attributed to the Si-Ge TO phonon replica. With respect to the no-phonon transitions, for the sample $S1$ ($S2$) and for I in the range from 0.15 to 0.40 W cm^{-2} (0.15 to 0.30 W cm^{-2}) a single profile with a fixed value of $E_0 =$ 888 meV ($E_0 = 832$ meV) was used. For I in the range from 0.49 to 0.62 W cm^{-2} (0.35 to 0.99 W cm^{-2}), a second profile with $E_0 = 893$ meV ($E_0 = 842$ meV) was added and another profile with $E_0 = 898$ meV ($E_0 = 848$ meV) was added for I in the range from 0.99 to 7.90 W cm^{-2} (1.48 to 3.95 W cm^{-2}). The purely electronic (no-phonon) transitions are attributed to the ground-state exciton (X_0), excited exciton (X_1), and ground-state biexciton (XX_0) in the case of $S1$ (see Fig. 2), and to X_0, XX_0, and excited biexciton state (XX_1) in the case of $S2$. This interpretation is based on the observed I dependence of the oscillator strengths F_i (see Sec. III B), and the results of electronic structure calculations (see Sec. III C).

TABLE I. Energies of the fitted GL profiles and calculated energies of the no-phonon excitons for samples $S1$ and $S2$ along with the energies of the phonon replicas taken from Fig. 8 of Ref. 29. The energies of the phonon replicas and the excitonic complexes are given relative to the corresponding value of X_0. The displayed values of the energies of the phonon replicas were taken from the corresponding GL profiles of the spectra for the lowest excitation intensities. The estimated uncertainties of the energies of the fitted GL bands are ~ 3 meV for the no-phonon bands and ~ 6 meV for the phonon-assisted ones. For the uncertainties of the calculated values of X_0 see the text; the uncertainty of the calculated energies of the other excitonic complexes is ~ 2 meV. The uncertainty of the phonon energies derived from Fig. 8 of Ref. 29 is ~ 1 meV.

	X_0	X_1	XX_0	XX_1	TO Si-Ge	TO Ge-Ge	LA	TA
$S1$ fit (meV)	888 ± 3	$+5 \pm 3$	$+10 \pm 3$		-52 ± 6	-39 ± 6	-26 ± 6	-9 ± 6
$S1$ theory (meV)	887 ± 20	$+7 \pm 2$	$+11 \pm 2$					
$S2$ fit (meV)	832 ± 3		$+10 \pm 3$	$+16 \pm 3$	-46 ± 6	-34 ± 6	-19 ± 6	-9 ± 6
$S2$ theory (meV)	837 ± 20	$+8 \pm 2$	$+12 \pm 2$	$+18 \pm 2$				
Ref. 29 (meV)					-49	-35	-30	-10

B. Excitation intensity dependence

The I dependencies of the oscillator strengths F_i and of the Gaussian full widths at half maximum (FWHM) of the fitted profiles of the no-phonon transitions are displayed in Fig. 4 and its insets, respectively. In order to suppress the uncertainties of the pumping intensities all F_i values shown in Fig. 4 for sample $S1$ [shown in panel (a)] [$S2$ [panel (b)]] are normalized to the oscillator strength of the 888 meV (832 meV) band, which corresponds to the lowest excitonic state (X_0, with F_{X_0} linear in I). Figure 4(a) reveals an approximately linear ($\sim I^{1.03}$) dependence of F of the 893 meV band and a superlinear ($\sim I^{2.09}$) dependence of the 898 meV band of the sample $S1$. For the sample $S2$, both the 842 meV band and the 848 meV one exhibit a superlinear ($\sim I^{1.70}$) and ($\sim I^{1.92}$) dependence of F, respectively, as shown in Fig. 4(b). [Note, that due to the linearity of the normalization factor F_{X_0} with respect to I, quadratic (linear) powers of I appear as linear (constant) functions in Fig. 4.]

Figure 4 also shows the I dependence of the sum of the oscillator strengths of the phonon replicas. This dependence is also slightly superlinear, $\sim I^{1.11}$ and $\sim I^{1.42}$ for $S1$ and $S2$, respectively. We interpret this finding as an indication for contributions of phonon replica lines of nonlinear exciton emissions. Note, that for the sample $S2$ the relative magnitude of the contribution to the phonon-replica bands superlinear in I is larger than for the sample $S1$. This may be due to the fact that the ratio of the sum of F for the no-phonon bands having a superlinear I dependence to that of those having a linear I dependence is higher for $S2$ than for $S1$. The broad features in the I dependence of F and FWHM (the latter shown in the inset of Fig. 4) are fitting artifacts caused by high correlations of the parameters F_i and $\Gamma_{G,i}$, respectively. Note, that the values of the FWHM of the no-phonon bands are comparable to the FWHM of the X_0 band observed for SiGe bulk crystals (8 meV; see Fig. 10 of Ref. 29). However, they are considerably larger for $S2$ than for $S1$ (by a factor of ~ 2).

The insets of Fig. 4 show that the differences between the various exciton resonance energies are comparable to the widths of the GL profiles, i.e., despite the excellent homogeneity of the QD ensemble these differences are just beyond the experimental resolution limit. Thus, any additional inhomogeneous line broadening, such as that occurring in randomly nucleated islands, hindered the discrimination of various excitonic contributions to the PL spectra in previous studies.

C. Electronic structure calculations

To get a better insight into the origin of the no-phonon transitions, a series of calculations of the electronic structure was performed using the following two-step approach. First, the single-particle wave functions were obtained by the nextnano++ solver[31] using the single-band effective Schrödinger equation for the electron states in the Δ valley of the lowest conduction band and the six-band envelope function method for the hole states. The electron and hole states were thus treated as decoupled. This approximation is justified considering the energy difference of ~ 750 meV between the extrema of the confinement potentials of electrons and holes. Second, these calculated wave functions were used to construct a basis set for the configuration interaction (CI) calculations.[32] The evaluation of the Coulomb matrix elements is facilitated by the orthogonality of the periodic parts of the Bloch waves of the bottom of the conduction band in Si and the top of the valence band in both Si and Ge.[33]

Next we describe the model structures. The SiGe QDs of sample $S1$ were defined on the rectangular grid and approximated by cones with a base diameter of 122.8 nm and a height of 15.3 nm as sketched in Fig. 5. For sample $S2$, a similar structure was used with slightly different dimensions of 118 and 15 nm deduced from the AFM measurements on uncapped islands. In the model structure representing the sample $S1$ ($S2$) the Ge content linearly increases from 0.277 (0.34) at the QD base to 0.43 (0.49) at its apex; this is motivated by results of Ref. 7. The Ge concentration profiles were chosen to warrant agreement between the measured and calculated values of the transition energy of the lowest no-phonon transition. For more information on the model structures, see Fig. 5; for the material parameters, see Tables II and III. We have found that the uncertainty in the values of the deformation potentials in Si and Ge (estimated from the spread of the values published in Refs. 34–37) leads to an uncertainty of ~ 20 meV in the calculated value of the energy of X_0. However, the differences between the energy of X_0 and those of the other excitonic complexes are almost independent of the choice of the deformation potential parameters. The spacing of the grid used in the calculations was set to 4 nm in both lateral

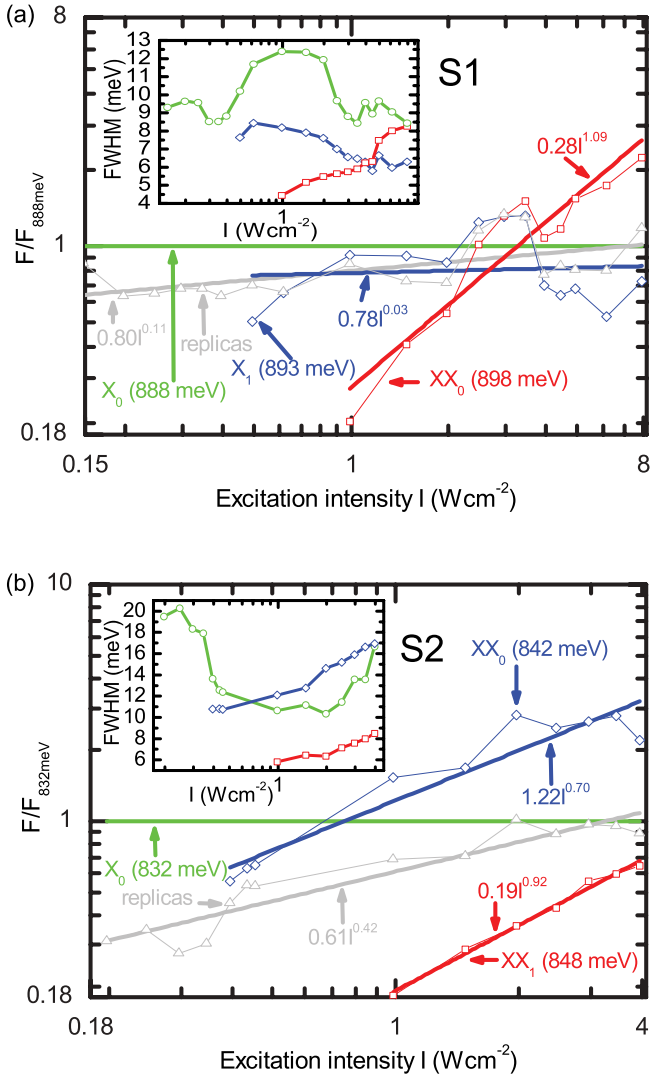

FIG. 4. (Color online) Excitation intensity (I) dependence of the oscillator strength (F_i) normalized to the respective squared resonance energies $E_{0,i}$ and divided by the oscillator strength F_{X_0} of the no-phonon transition with the lowest value of E_0, i.e., of the X_0 profile, for the no-phonon transition GL profiles in the sample $S1$ (a) and in the sample $S2$ (b). The sums of F_i of the phonon replicas are displayed by open triangles. The thick lines represent fits of the measured data to the linear functions $a_1 I^{a_2}$ and the thin ones are guides to the eye. Note, that due to the linearity of the normalization factor F_{X_0} with respect to I, quadratic (linear) powers of I appear as linear (constant) functions. The graphs in the insets show the I dependence of the FWHM of the fitted Gaussian lines. The same symbols as in the main diagram are used except for the dependencies of the profiles with the lowest value of E_0, which are displayed by open circles.

and vertical directions except for a cuboid around the QD apex (shown in Fig. 5 by the broken line) where the spacing was 0.5 nm in all directions. The Schrödinger equation was solved only in this subspace owing to the expected positions of the electron and hole states.[38] On the other hand, the minimization of the strain energy was performed in the whole simulation space. For both calculations von Neumann boundary conditions were used in both lateral and vertical directions.

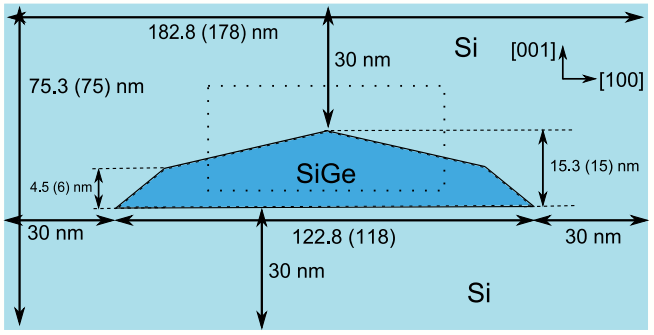

FIG. 5. (Color online) A cut through the simulation space for the SiGe QD of sample $S1$ ($S2$), containing its vertical axis. The QDs were approximated by cylindrically symmetric cones with the dimensions shown in the figure. The Ge content inside the QD varies linearly from 0.277 (0.34) at the base of the cone to 0.43 (0.49) at its apex. The dotted rectangle denotes the space where the Schrödinger equation was solved and the grid spacing was set to 0.5 nm.

D. Assignment of the PL bands

The calculated values of the transition energies of the states X_0, X_1, and XX_0 for the sample $S1$ are indicated in Fig. 2 by the broken and full vertical lines along with the probability densities of the single-electron wave functions [inset of panel (c)]. Note that for both samples the hole wave functions were predominantly composed of heavy holes (96%); the electron wave functions, from which the lowest excitonic (and biexcitonic) states were composed, belonged purely to the lower-lying Δ_z conduction-band valleys oriented with their main axis along the [001] growth direction. This is due to the difference of $\sim$18 meV between the energies of the lowest Δ_z and the four Δ_{xy} single-electron states and almost no spatial overlap between the Δ_{xy} state and the hole states (these results have been obtained by calculations involving the whole simulation space with a less dense grid).[38]

The resulting energy of the excitonic ground state (X_0) for the sample $S1$, calculated using the CI method with six electron and four hole basis states, was found to be 887 meV (the corresponding single-particle energy difference between the electron and hole states is 896 meV), close to the observed value of 888 meV, and that of the first excited excitonic state (X_1) was found to be 894 meV. The biexciton (XX_0) was found to be shifted to higher energies with respect to the exciton ground state by 11 meV, a value which is in very good agreement with the experimentally observed energy difference of 10 meV between the first and the third no-phonon GL profiles having the linear and a superlinear I dependence of F, respectively. Also the observed difference of 5 meV between the energies of the first and second no-phonon profiles is in reasonable agreement with the calculated value of $E(X_1) - E(X_0)$ of 7 meV. Thus, we assign the 888 and 893 meV profiles to the recombination of X_0 and X_1, respectively, and the 898 meV profile to the recombination of XX_0. This assignment is corroborated by the observed dependence of the strength of the respective GL profiles on I as discussed in Sec. III B.

For the sample $S2$, the energy of X_0, calculated using the CI method with six electron and four hole basis states, was

TABLE II. Description of the material parameters used in the calculations γ_1, γ_2, and γ_3 are the Luttinger parameters (Ref. 41).

Parameter	Description
a	Lattice constant
a_{exp}	Lattice thermal expansion coefficient
C_{11}	Elastic constant
C_{12}	Elastic constant
C_{44}	Elastic constant
ε_r	Static dielectric constant
$m_{\Delta l}$	Δ-valley longitudinal electron effective mass
$m_{\Delta t}$	Δ-valley transversal electron effective mass
E_0	Band gap
α	Varshni parameter
β	Varshni parameter
E_v	Valence-band offset
Δ_0	Spin-orbit split-off energy
a_c	Absolute deformation potential for conduction-band Δ valley
a_u	Uniaxial shear deformation potential of the conduction-band Δ valley
a_v	Absolute deformation potential for valence band
a_{ub}	Uniaxial shear deformation potential b of the valence bands
a_{ud}	Uniaxial shear deformation potential d of the valence bands
L	Dresselhaus parameter (Ref. 42); $L = -\gamma_1 - 4\gamma_2 - 1$
M	Dresselhaus parameter (Ref. 42); $M = 2\gamma_2 - \gamma_1 - 1$
N	Dresselhaus parameter (Ref. 42); $N = -6\gamma_3$

found to be 837 meV (the corresponding single-particle energy difference between the electron and hole states is 847 meV), close to the observed value of 832 meV. The calculated values of the blueshift of the biexciton ground state XX_0 and of the biexciton excited state XX_1 are 12 and 18 meV, respectively, in good agreement with the experimentally observed energy differences of 10 and 16 meV between the second and the first no-phonon band, and between the third and the first no-phonon band, respectively. Thus, we attribute the 832, 842, and 848 meV bands to the recombination of X_0, XX_0, and XX_1, respectively, again in agreement with the observed dependence of their strength on I as discussed in Sec. III B. The excited excitonic state X_1 observed in sample $S1$ was not identified here. This is probably due to the larger inhomogeneous broadening of the GL profiles in $S2$ compared to $S1$. The X_1 band might contribute to the second no-phonon profile, causing

TABLE III. Values of the material parameters used in the calculations. The unit m_0 represents the free electron mass.

Parameter	Unit	Si	Ge	$Si_{1-x}Ge_x$
a	Å	5.4304 (Ref. 43)	5.6579 (Ref. 43)	Linear
a_{exp}	Å/K	1.8138×10^{-5} (Ref. 43)	5.8×10^{-5} (Ref. 44)	Linear
C_{11}	GPa	165.77 (Ref. 43)	128.53 (Ref. 43)	Linear
C_{12}	GPa	63.93 (Ref. 43)	48.26 (Ref. 43)	Linear
C_{44}	GPa	79.62 (Ref. 43)	66.80 (Ref. 43)	Linear
ε_r		11.7 (Ref. 45)	16.2 (Ref. 43)	Linear
$m_{\Delta l}$	m_0	0.916 (Ref. 45)	1.350 (Ref. 31)	Linear
$m_{\Delta t}$	m_0	0.190 (Ref. 45)	0.290 (Ref. 31)	Linear
E_0	eV	1.17 (Ref. 46)	0.931 (Ref. 29)	$0.931x + 1.17(1-x)$ $-0.206x(1-x)$ (Ref. 29)
α	eV/K	0.473×10^{-3} (Ref. 44)	0.4774×10^{-3} (Ref. 31)	Linear
β	K	636 (Ref. 44)	235 (Ref. 31)	Linear
E_v	eV	1.090 (Ref. 37)	1.67 (Ref. 37)	Linear
Δ_0	eV	0.044 (Ref. 43)	0.30 (Ref. 43)	Linear
a_c	eV	3.40 (Ref. 37)	0.14 (Ref. 37)	Linear
a_u	eV	9.16 (Ref. 35)	9.42 (Ref. 35)	Linear
a_v	eV	2.05 (Ref. 37)	−0.35 (Ref. 37)	Linear
a_{ub}	eV	−2.10 (Ref. 47)	−2.86 (Ref. 48)	Linear
a_{ud}	eV	−4.85 (Ref. 47)	−5.28 (Ref. 48)	Linear
L	$\hbar^2/2m_0$	−6.69 (Ref. 49)	−31.34 (Ref. 50)	Linear
M	$\hbar^2/2m_0$	−4.62 (Ref. 49)	−5.90 (Ref. 50)	Linear
N	$\hbar^2/2m_0$	−8.56 (Ref. 49)	−34.14 (Ref. 50)	Linear

a slightly lower magnitude of its superlinear I dependence seen in Fig. 4(b). Also, excited-state surface trapping, as observed in Ref. 24 for colloidal nanocrystals, might quench more efficiently the X_1 emission in $S2$ as compared to $S1$ due to the thinner capping layer of $S2$. The assignment of the 842 and 848 meV bands to XX_0 and XX_1 is not unique as a similarly satisfying agreement with the experimental data may be achieved by attributing these to the recombination of the ground-state trion and a XX_0 at an even higher energy, respectively. However, in our calculations this would require the assumption of a Ge concentration profile in the QD, with an—for the ordered SiGe QDs—unrealistically large Ge accumulation of up to 60%–70% at its apex. Evidence for such a large Ge concentration in the apex of a SiGe transition dome and dome islands have been found up to now only in randomly nucleated islands grown on planar substrates, but not in ordered ones.[6,7,39]

Our calculations and experiments show that the exciton-exciton interaction is pronouncedly antibinding in SiGe QDs, resulting in $\sim$10 meV higher biexciton transition energies as compared to the exciton ones. A similar antibinding exciton-exciton interaction was invoked in the interpretation of Ge hut-cluster absorption spectra.[4] Since also in InAs/GaAsSb,[22] GaSb/GaAs,[20] and in InP/GaAs[21] quantum dot systems with type-II band alignment a large antibinding exciton-exciton interaction was found, we conclude that the antibinding character of the exciton-exciton interaction is characteristic of type-II systems with spatially separated electrons and holes.[22,40] Our conclusion is also supported by extensive work on exciton-exciton repulsion in colloidal semiconductor nanocrystals reported in Refs. 23 and 26.

IV. CONCLUSIONS

In conclusion, we have performed extensive intensity-dependent PL measurements on two ensembles of two dimensionally ordered SiGe QDs, whose excellent homogeneity is due to the controlled growth on prepatterned Si substrates. The spectra were decomposed into a series of distinct bands with characteristic excitation intensity dependencies of their oscillator strengths. Electronic structure calculations were performed using the nextnano++ solver and the calculated wave functions were used as a basis set for configuration interaction calculations. Based on these calculations, the transition energies of the X_0, X_1, XX_0, and XX_1 states were compared with the experimentally observed PL bands. Together with the experimentally observed excitation intensity dependence of the various PL bands, the excitonic and biexcitonic recombinations are identified in this type-II quantum dot system. The determined exciton interaction and excited-state energies are important for the application of SiGe QDs in Si photonics.

ACKNOWLEDGMENTS

The authors thank M. Grydlik for her help with designing the growth of the ordered QDs. P.K. would like to thank the ÖAD Stipendium "Aktion Österreich–Tschechien" and the NANOE Project No. CZ.1.07/2.3.00/20.0027 for financing his research stay in Linz. This work was supported by the project "CEITEC–Central European Institute of Technology" (CZ.1.05/1.1.00/02.0068) from European Regional Development Fund, the internal project MUNI/A/1047/2009, the Austrian Nanoinitiative (FFG, Grants No. 815802 and No. 815803), the IRON Projects No. SFB025-02 and No. SFB025-12 (FWF), and GMe, Austria.

*klenovsky@physics.muni.cz

[1] L. Tsybeskov and D. J. Lockwood, Proc. IEEE **97**, 1284 (2009).
[2] Y. W. Mo, D. E. Savage, B. S. Swartzentruber, and M. G. Lagally, Phys. Rev. Lett. **65**, 1020 (1990).
[3] D. J. Eaglesham and M. Cerullo, Phys. Rev. Lett. **64**, 1943 (1990).
[4] A. I. Yakimov, N. P. Stepina, A. V. Dvurechenskii, A. I. Nikiforov, and A. V. Nenashev, Phys. Rev. B **63**, 045312 (2001).
[5] A. Yakimov, N. Stepina, A. Dvurechenskii, A. Nikiforov, and A. Nenashev, Physica E **13**, 1026 (2002).
[6] A. Rastelli, M. Stoffel, A. Malachias, T. Merdzhanova, G. Katsaros, K. Kern, T. H. Metzger, and O. G. Schmidt, Nano Lett. **8**, 1404 (2008).
[7] M. Brehm, M. Grydlik, F. Hackl, E. Lausecker, T. Fromherz, and G. Bauer, Nanoscale Res. Lett. **5**, 1868 (2010).
[8] J. Wan, G. Jin, Z. Jiang, Y. Luo, J. Liu, and K. Wang, Appl. Phys. Lett. **78**, 1763 (2001).
[9] M. Dashiell, U. Denker, and O. Schmidt, Appl. Phys. Lett. **79**, 2261 (2001).
[10] M. L. W. Thewalt, D. A. Harrison, C. F. Reinhart, J. A. Wolk, and H. Lafontaine, Phys. Rev. Lett. **79**, 269 (1997).
[11] C. Penn, F. Schäffler, G. Bauer, P. C. M. Christianen, J. C. Maan, and S. Glutsch, Phys. Rev. B **61**, 13055 (2000).
[12] C. Penn, F. Schäffler, G. Bauer, and S. Glutsch, Phys. Rev. B **59**, 13314 (1999).
[13] Z. Zhong, A. Halilovic, T. Fromherz, F. Schäffler, and G. Bauer, Appl. Phys. Lett. **82**, 4779 (2003).
[14] T. Stoica, V. Shushunova, C. Dais, H. Solak, and D. Grützmacher, Nanotechnology **18**, 455307 (2007).
[15] E. Lausecker, M. Brehm, M. Grydlik, F. Hackl, I. Bergmair, M. Mühlberger, T. Fromherz, F. Schäffler, and G. Bauer, Appl. Phys. Lett. **98**, 143101 (2011).
[16] F. Hackl, M. Grydlik, M. Brehm, H. Groiss, F. Schäffler, T. Fromherz, and G. Bauer, Nanotechnology **22**, 165302 (2011).
[17] M. Skolnick and D. Mowbray, Annu. Rev. Mater. Res. **34**, 181 (2004).
[18] G. A. Narvaez, G. Bester, and A. Zunger, Phys. Rev. B **72**, 245318 (2005).
[19] A. Schliwa, M. Winkelnkemper, and D. Bimberg, Phys. Rev. B **79**, 075443 (2009).
[20] K. Matsuda, S. V. Nair, H. E. Ruda, Y. Sugimoto, T. Saiki, and K. Yamaguchi, Appl. Phys. Lett. **90**, 013101 (2007).
[21] B. Bansal, S. Godefroo, M. Hayne, G. Medeiros-Ribeiro, and V. V. Moshchalkov, Phys. Rev. B **80**, 205317 (2009).
[22] P. Klenovský, V. Křápek, D. Munzar, and J. Humlíček, Appl. Phys. Lett. **97**, 203107 (2010).

[23]Z. Deutsch, A. Avidan, I. Pinkas, and D. Oron, Phys. Chem. Chem. Phys. **13**, 3210 (2011).
[24]P. Kambhampati, J. Phys. Chem. C **115**, 22089 (2011).
[25]P. Kambhampati, J. Phys. Chem. Lett. **3**, 1182 (2012).
[26]V. I. Klimov, S. A. Ivanov, J. Nanda, M. Achermann, I. Bezel, J. A. McGuire, and A. Piryatinski, Nature (London) **447**, 441 (2007).
[27]M. Brehm, M. Grydlik, H. Groiss, F. Hackl, F. Schäffler, T. Fromherz, and G. Bauer, J. Appl. Phys. **109**, 123505 (2011).
[28]J. Humlíček, E. Schmidt, L. Bočánek, R. Švehla, and K. Ploog, Phys. Rev. B **48**, 5241 (1993).
[29]J. Weber and M. I. Alonso, Phys. Rev. B **40**, 5683 (1989).
[30]J. C. Sturm, H. Manoharan, L. C. Lenchyshyn, M. L. W. Thewalt, N. L. Rowell, J. P. Noel, and D. C. Houghton, Phys. Rev. Lett. **66**, 1362 (1991).
[31]S. Birner, T. Zibold, T. Andlauer, T. Kubis, M. Sabathil, A. Trellakis, and P. Vogl, IEEE Trans. Electron Devices **54**, 2137 (2007).
[32]S. Rodt, A. Schliwa, K. Potschke, F. Guffarth, and D. Bimberg, Phys. Rev. B **71**, 155325 (2005).
[33]M. Cardona and F. Pollak, Phys. Rev. **142**, 530 (1966).
[34]C. G. Van de Walle, Phys. Rev. B **39**, 1871 (1989).
[35]C. G. Van de Walle and R. M. Martin, Phys. Rev. B **34**, 5621 (1986).
[36]G. S. Cargill, J. Angilello, and K. L. Kavanagh, Phys. Rev. Lett. **61**, 1748 (1988).
[37]S. Wei and A. Zunger, Appl. Phys. Lett. **72**, 2011 (1998).
[38]M. Brehm, T. Suzuki, T. Fromherz, Z. Zhong, N. Hrauda, F. Hackl, J. Stangl, F. Schäffler, and G. Bauer, New J. Phys. **11**, 063021 (2009).
[39]T. U. Schülli, G. Vastola, M.-I. Richard, A. Malachias, G. Renaud, F. Uhlik, F. Montalenti, G. Chen, L. Miglio, F. Schäffler, and G. Bauer, Phys. Rev. Lett. **102**, 025502 (2009).
[40]A. Yoffe, Adv. Phys. **50**, 1 (2001).
[41]J. Luttinger, Phys. Rev. **102**, 1030 (1956).
[42]G. Dresselhaus, A. Kip, and C. Kittel, Phys. Rev. **98**, 368 (1955).
[43]H. Hans Landolt, R. Börnstein, K. H. Hellwege, Dieter Bimberg, M. Schulz, H. Weiss, O. Madelung *et al.*, *Landolt-Börnstein, Numerical Data and Functional Relationships in Science and Technology*, Group 3, Crystal and Solid State Physics, Vol. 17, Semiconductors (Springer, Berlin, 1982).
[44]S. M. Sze, *Physics of Semiconductor Devices*, Vol. II (Wiley, New York, 1981).
[45]K. W. Boer, *Survey of Semiconductor Physics*, Vol. II (Wiley, New York, 1990).
[46]See www.ioffe.rssi.ru/SVA/NSM/Semicond/Si/bandstr.html.
[47]L. Laude, F. Pollak, and M. Cardona, Phys. Rev. B **3**, 2623 (1971).
[48]M. Chandrasekhar and F. Pollak, Phys. Rev. B **15**, 2127 (1977).
[49]M. M. Rieger and P. Vogl, Phys. Rev. B **48**, 14276 (1993).
[50]J. Hensel and K. Suzuki, Phys. Rev. B **9**, 4219 (1974).